Time-Optimal Control of Gravity-Gradient Satellites with Disturbances

FRANZ C. ZACH*
NASA Goddard Space Flight Center, Greenbelt, Md.

Attitude control of spacecraft with coarse stabilization by the gravity-gradient technique plus active libration damping for precise pointing represents a promising approach for advanced experiments, e.g., laser communications. This paper deals with the time optimal control (acquisition of precise pointing) for this case. A near optimal control law for the general Gravity-Gradient Satellite (GGS) is obtained by making two approximations: 1) the general GGS is approximated by a Dumbbell Satellite (DS) and 2) a small-angle approximation. The optimal control law for this case is calculated and then applied to two representative examples of a synchronous GGS. The Maximum Principle is used and is extended to cover operating conditions with disturbances. It is shown that disturbances change the optimal control law significantly, a result that is very important for practical applications of the Maximum Principle.

Nomenclature†

a_α, a_ϕ, a_ψ = gravity-gradient coefficient for pitch, roll, and yaw, respectively
C_1 = linear viscous damping coefficient of the damper rod
C_2 = linear spring coefficient of the damper rod
d_i = reduced disturbance torque ($= T_{di}/I_{ii}$), $i = x,y,z$
DS = Dumbbell Satellite
GG = Gravity Gradient; GGS = Gravity Gradient Satellite
H_{ib} = inertial angular momentum of the main body of the spacecraft, measured in body-fixed coordinates, $i = x,y,z$
I_l = moment of inertia of the damper rod about its axis of rotation
$[I]$ = inertia tensor of the main spacecraft body
r = distance from the center of the Earth to the c.m. of the spacecraft
t = time
T_{ci}, T_{di} = control and disturbance torques, respectively, $i = x,y,z$
u_i = reduced control torques ($= T_{ci}/I_{ii}$), $i = x,y,z$
v = inertial velocity of the spacecraft
x_0,y_0,z_0 = attitude reference system (x_0 has the direction from the center of the earth to the c.m. of the spacecraft, y_0 lies normal to x_0 and in the orbital plane such that the component of v in the y_0 direction is greater than zero, z_0 is perpendicular to the orbit plane)
x_b,y_b,z_b = coordinate system fixed to the main body of the spacecraft (x_b — yaw axis, y_b — roll axis, z_b — pitch axis)
x_d,y_d,z_d = coordinate system fixed to the damper rod
α = pitch angle; α_s = set value of α
μ = Earth gravitational constant
ξ_{ib} = orbital angular rate, i.e., rotation of the x_0,y_0,z_0 system in inertial space, measured in the x_b,y_b,z_b system, $i = x,y,z$
ρ_1, ρ_2 = angles of the damper rod relative to the body-fixed coordinate system
τ = time consumed for damping of initial librations
ϕ = roll angle; ϕ_s = set value of ϕ
ψ = yaw angle
Ω_{ib} = inertial angular velocity of the main body of the spacecraft, measured in the x_b,y_b,z_b-system, $i = x,y,z$
ω_0 = orbital angular rate for a circular orbit [$= (\mu/r^3)^{1/2}$]

Received March 11, 1970; revision received July 31, 1970. The work for this paper was accomplished while the author held a National Research Council Postdoctoral Resident Research Associateship supported by the NASA Goddard Space Flight Center. The author is very much obliged to W. Isley and D. Endres for their valuable suggestions.

* Research Associate, Auxiliary Propulsion Branch, NASA Goddard Space Flight Center. Member AIAA.

† All coordinate systems are centered at the center of mass (c.m.) of the spacecraft and are right-handed.

Introduction

THE development of control policies for precise pointing of spacecraft is needed for advanced experiments, e.g., laser communications. The Gravity Gradient (GG) technique[1,2] offers a good approach for long-term, coarse stabilization of a spacecraft. However, the over-all optimal control policy must meet two basic objectives: 1) acquisition of the precision pointing mode in minimum time starting from a coarse GG mode (generally in the presence of disturbances and 2) extended term precision pointing by counteraction of disturbance torques. This paper treats only the acquisition requirement. The optimal control law as developed herein is applied to two representative examples of a synchronous equatorial (24-hr) Earth satellite using small (micropound thrust) reaction jet devices for active libration damping. Use of ion engines as the thrusters would require special consideration of control actuations, because ion engines cannot be turned on and off readily. One possibility is to combine libration damping with orbit corrections; another is to provide a balanced couple which cancels out the orbital effects. The use of resistojets[3] has already been studied as a means of optimal large angle maneuvering. Pulsed plasma systems appear to offer promise for use in both acquisition and holding modes due to their precision impulse bit capability and relatively high specific impulse. It is assumed that a minimum of six thrust directions is provided on the spacecraft to provide control in pitch, roll, and yaw axes.

Efforts have been made in the literature to apply optimal control concepts to spacecraft. In Ref. 3, time and fuel optimal control policies are derived and investigated for the case of active 3 axes attitude control of synchronous communication satellites by means of microthrusters. Reference 7 treats active time optimal angular velocity control of spinning space bodies. In Ref. 8, an approximate solution for the fuel optimal control of a DS is derived. In the work presented here a time optimal attitude control procedure is proposed which combines active control by means of microthrusters with the passive GG concept.

The procedure used to develop these control laws is as follows: 1) the general rotational equations of motion for a GGS with rigid structure including a single-degree-of-freedom damper rod are formulated; 2) assuming small attitude librations and the pitch moment of inertia approximately equal to the sum of the two other principal moments of inertia,‡ these equations are linearized for the case of a symmetric, undamped satellite (=DS) configuration in a circular equatorial orbit; and 3) the optimal control laws are developed for this DS. To check the validity of these control laws for a more general synchronous GGS, the control laws are applied to the simulation of the complete GGS.

Equations of Motion for a GGS

The equations of motion of a GGS with rigid structure and a single-degree-of-freedom damper rod (Fig. 1) are[1]

$$[I]\begin{pmatrix}\dot{\Omega}_{xb}\\ \dot{\Omega}_{yb}\\ \dot{\Omega}_{zb}\end{pmatrix} = \begin{pmatrix}\delta_{xb}\\ \delta_{yb}\\ \delta_{zb}\end{pmatrix} \tag{1}$$

where

$$\delta_{xb} = M_{xb} + M_{xd}\sin\rho_2 + M_{zd}\cos\rho_2 - (\Omega_{yb}H_{zb} - \Omega_{zb}H_{yb}) - P\cos\rho_2 + T_{cx} + T_{dx} \tag{2}$$

$$\delta_{yb} = M_{yb} + M_{xd}\cos\rho_2\cos\rho_1 + M_{SD}\sin\rho_1 - M_{zd}\sin\rho_2 \times \cos\rho_1 - (\Omega_{zb}H_{xb} - \Omega_{xb}H_{zb}) + P\sin\rho_2 \times \cos\rho_1 + T_{cy} + T_{dy} \tag{3}$$

$$\delta_{zb} = M_{zb} + M_{xd}\cos\rho_2\sin\rho_1 - M_{SD}\cos\rho_1 - M_{zd}\sin\rho_2\sin\rho_1 - (\Omega_{xb}H_{yb} - \Omega_{yb}H_{xb}) + P\sin\rho_2\sin\rho_1 + T_{cz} + T_{dz} \tag{4}$$

The torques M_{ib} and M_{id} caused by the GG effect are: for the main body of the spacecraft

$$M_{xb} = -3\mu[(I_{yy} - I_{zz})a_2a_3 + I_{xy}a_1a_3 - I_{xz}a_1a_2 + I_{yz}(a_3^2 - a_2^2)]/r^3 \tag{5}$$

$$M_{yb} = -3\mu[(I_{zz} - I_{xx})a_1a_3 - I_{xy}a_2a_3 + I_{xz}(a_1^2 - a_3^2) + I_{yz}a_1a_2]/r^3 \tag{6}$$

$$M_{zb} = -3\mu[(I_{xx} - I_{yy})a_1a_2 + I_{xy}(a_2^2 - a_1^2) + I_{xz}a_2a_3 - I_{yz}a_1a_3]/r^3 \tag{7}$$

and for the damper rod

$$M_{xd} = 0,\ M_{yd} = -3\mu I_l b_1 b_2/r^3 \tag{8}$$

$$M_{zd} = 3\mu I_l b_1 b_3/r^3 \tag{9}$$

P and M_{SD} used in Eqs. (2–4) are given by

$$P = I_l\Omega_{xd}(\Omega_{yd} - \dot{\rho}_2) \tag{10}$$

$$M_{SD} = C_1\rho_2 + C_2\dot{\rho}_2 \tag{11}$$

where the latter term is the restoring torque exerted on the damper rod by the spring-damper mechanism. P is used for abbreviation purposes.

The $a_i(i = 1,2,3)$ and $b_i(i = 1,2,3)$ used in Eqs. (5–9), which give the relations of the GG torque to the angular positions, are

$$a_1 = \cos\alpha\cos\phi \tag{12}$$

$$a_2 = \cos\alpha\sin\phi\sin\psi + \sin\alpha\cos\psi \tag{13}$$

$$a_3 = -\cos\alpha\sin\phi\cos\psi + \sin\alpha\sin\psi \tag{14}$$

$$b_1 = a_1\sin\rho_2 + a_2\cos\rho_2\cos\rho_1 + a_3\cos\rho_2\sin\rho_1 \tag{15}$$

$$b_2 = -a_2\sin\rho_1 + a_3\cos\rho_1 \tag{16}$$

$$b_3 = a_1\cos\rho_2 - a_2\sin\rho_2\cos\rho_1 - a_3\sin\rho_2\sin\rho_1 \tag{17}$$

‡ This assumption is valid, e.g., for the ATS-D/E spacecraft.[9]

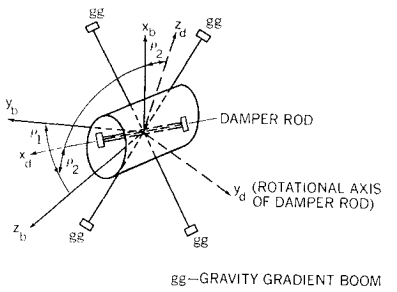

Fig. 1 GGS x_b and y_b lie in the plane of the four booms and together with z_b establish a right-handed coordinate system fixed to the main body of the spacecraft; x_d,y_d,z_d establish a right-handed coordinate system fixed to the damper rod.

The equation of motion for the damper rod is

$$\ddot{\rho}_2 = -\dot{\Omega}_{yb}\sin\rho_1 + \dot{\Omega}_{zb}\cos\rho_1 - \Omega_{zd}\Omega_{xd} - (M_{yd} + M_{SD})/I_l \tag{18}$$

Integration of Eqs. (1) and (18) furnishes Ω_{xb}, Ω_{yb}, Ω_{zb}, and ρ_2.

The pitch, roll, and yaw angles, which are the Euler angles between the body-fixed and the attitude reference system, will be used throughout this report. The Euler angle rates can be obtained by subtracting ξ_b, the rate at which the attitude reference system rotates relative to the inertial system, from $\boldsymbol{\Omega}_b$. This gives

$$\dot{\alpha} = (\cos\phi)^{-1}[(\Omega_{yb} - \xi_{yb})\sin\psi + (\Omega_{zb} - \xi_{zb})\cos\psi] \tag{19}$$

$$\dot{\phi} = -(\Omega_{yb} - \xi_{yb})\cos\psi + (\Omega_{zb} - \xi_{zb})\sin\psi \tag{20}$$

and

$$\dot{\psi} = \Omega_{xb} - \xi_{xb} - \dot{\alpha}\sin\phi \tag{21}$$

A digital computer program was written[1] for the calculation of α, ϕ, ψ, and ρ_2 according to Eqs. (1–21). This program also includes elastic collision processes of the damper rod against its stops, which limits the rotation of the damper rod in the $x_d - z_d$ plane.

Approximation of GGS by a DS

For a DS, it will be assumed that no damper rod exists and that

$$I_{yy} \approx I_{zz} \gg I_{xx} \tag{22}$$

Equations (1–4) now yield:

$$I_{xx}\dot{\Omega}_{xb} = (I_{yy} - I_{zz})\Omega_{yb}\Omega_{zb} + T_{cx} + T_{dx} + M_{xb} \tag{23}$$

$$I_{yy}\dot{\Omega}_{yb} = (I_{zz} - I_{xx})\Omega_{zb}\Omega_{xb} + T_{cy} + T_{dy} + M_{yb} \tag{24}$$

$$I_{zz}\dot{\Omega}_{zb} = (I_{xx} - I_{yy})\Omega_{xb}\Omega_{yb} + T_{cz} + T_{dz} + M_{zb} \tag{25}$$

Equations (5–9) become

$$M_{xb} = -3\mu(I_{yy} - I_{zz})a_2a_3/r^3 \tag{26}$$

$$M_{yb} = -3\mu(I_{zz} - I_{xx})a_1a_3/r^3 \tag{27}$$

$$M_{zb} = -3\mu(I_{xx} - I_{yy})a_1a_2/r^3 \tag{28}$$

$$M_{xd} = M_{yd} = M_{zd} = 0 \tag{29}$$

For small angles Eqs. (23–29) can be approximated[4] by

$$\ddot{\psi} + \omega_0^2\frac{I_{zz} - I_{yy}}{I_{xx}}\psi - \frac{I_{zz} - I_{yy} - I_{xx}}{I_{xx}}\omega_0\dot{\phi} = \frac{T_{cx} + T_{dx}}{I_{xx}} \tag{30}$$

$$\ddot{\phi} + 4\omega_0^2\frac{I_{zz} - I_{xx}}{I_{yy}}\phi + \frac{I_{zz} - I_{xx} - I_{yy}}{I_{yy}}\omega_0\dot{\psi} = \frac{T_{cy} + T_{dy}}{I_{yy}} \tag{31}$$

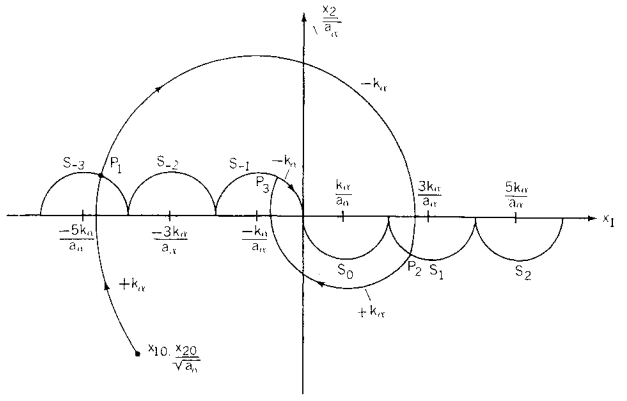

Fig. 2 Switching lines S_{-3}, S_{-2}, S_{-1}, S_0, S_1, S_2, with a trajectory starting from (x_{10}, $x_{20}/a_\alpha^{1/2}$). The switching points for the particular example illustrated are P_1, P_2, and P_3.

and

$$\ddot{\alpha} + 3\omega_0^2 \frac{I_{yy} - I_{xx}}{I_{zz}} \alpha = \frac{T_{cz} + T_{dz}}{I_{zz}} \tag{32}$$

where $\omega_0^2 = \mu/r^3 \approx \xi_{zb}^2$ and $\xi_{xb} \approx \xi_{yb} \approx 0$ for a nearly circular equatorial orbit. The sign on the right side of Eq. (31) is changed with respect to Eq. (24); this means that torques about the y axis are considered negative. This approach leads to a more convenient form for the derivation of the following optimal control concepts.

It is now assumed that

$$I_{zz} \approx I_{yy} + I_{xx} \tag{33}$$

Thus Eqs. (30–32) become

$$\ddot{\psi} + a_\psi \psi = u_\psi + d_\psi \tag{34}$$

$$\ddot{\phi} + a_\phi \phi = u_\phi + d_\phi \tag{35}$$

$$\ddot{\alpha} + a_\alpha \alpha = u_\alpha + d_\alpha \tag{36}$$

where

$$a_\psi = \omega_0^2(I_{zz} - I_{yy})/I_{xx},\ a_\phi = 4\omega_0^2(I_{zz} - I_{xx})/I_{yy} \tag{37}$$

$$a_\alpha = 3\omega_0^2(I_{yy} - I_{xx})/I_{zz} \tag{38}$$

$$u_\psi = (T_{cx}/I_{xx}),\ u_\phi = (T_{cy}/I_{yy}),\ u_\alpha = (T_{cz}/I_{zz}) \tag{39}$$

$$d_\psi = (T_{dx}/I_{xx}),\ d_\phi = (T_{dy}/I_{yy}) \text{ and } d_\alpha = (T_{dz}/I_{zz}) \tag{40}$$

When $d_\psi = d_\phi = d_\alpha = 0$ and u_ψ, u_ϕ, u_α are constant, Eqs. (34–36) give ellipses for each of the phase plane plots $(\psi,\dot{\psi})$, $(\phi,\dot{\phi})$ or $(\alpha,\dot{\alpha})$, respectively. Simulations of the GGS under the same conditions result in ellipses for the phase plane trajectories for angles up to 10°. This shows that results for the DS are applicable to the more general problem of the GGS. In order to apply available optimal control laws, the phase planes $[\psi,\dot{\psi}/(a_\psi)^{1/2}]$, $[\phi,\dot{\phi}/(a_\phi)^{1/2}]$ and $[\alpha,\dot{\alpha}/(a_\alpha)^{1/2}]$ are considered. The phase plots in these planes are circles for which optimal control laws given in Refs. 5, 7, and 10 are applicable.

Optimal Control for the DS

Equations (34–36) give a set of decoupled equations for pitch, yaw, and roll angles of a DS. These equations make the derivation of an optimal control law for nulling $\alpha,\dot{\alpha}$, $\phi,\dot{\phi},\psi$ and $\dot{\psi}$ using Pontryagin's Maximum Principle immediate. It is assumed that the reduced control torques u_α,u_ϕ, and u_ψ are bounded in magnitude, i.e.,

$$|u_i| \leq k_i, i = \alpha,\phi,\psi \tag{41}$$

Optimal Control Laws for Pitch (α) with No Disturbance Torques

The Maximum Principle[5,7,10] shows that for linear systems of order n with bounded control inputs the following procedure leads to the time optimal solution: a) The mathematical model of the system has to be written in the form of first-order linear differential equations

$$\dot{x}_i = f_i(\mathbf{x},\mathbf{u}) \tag{42}$$

where $\mathbf{x}$ is the vector of the state variables $(x_1 \ldots x_n)$ and $\mathbf{u}$ is the vector of the control variables $(u_1 \ldots u_n)$. b) The Hamiltonian

$$H = \sum_{i=1}^{n} p_i f_i(\mathbf{x},\mathbf{u}) \tag{43}$$

has to be maximized where $p_1 \ldots p_n$ are auxilliary variables given by

$$dp_i/dt = -\partial H/\partial x_i (i = 1,2 \ldots n) \tag{44}$$

and, from Eqs. (42) and (43)

$$dx_i/dt = \partial H/\partial p_i (i = 1,2, \ldots n) \tag{45}$$

In our case

$$\mathbf{x} = \begin{bmatrix} x_1 \\ x_2 \end{bmatrix} = \begin{bmatrix} \alpha \\ \dot{\alpha} \end{bmatrix} \tag{46}$$

$$\dot{\mathbf{x}} = \begin{bmatrix} \dot{x}_1 \\ \dot{x}_2 \end{bmatrix} = \begin{bmatrix} x_2 \\ -ax_1 + u_\alpha \end{bmatrix} \tag{47}$$

when $d_\alpha = 0$. Equation (43) yields

$$H = p_1 x_2 + p_2(-a_\alpha x_1 + u_\alpha) \tag{48}$$

which is maximized by

$$u_\alpha = k_\alpha \operatorname{sgn}[p_2] \tag{49}$$

Equation (44) leads to

$$\dot{p}_1 = a_\alpha p_2,\ \dot{p}_2 = -p_1 \tag{50}$$

Solving (50) gives

$$p_1 = -A a_\alpha^{1/2} \cos(a_\alpha^{1/2} t - \varphi) \tag{51}$$

$$p_2 = A \sin(a_\alpha^{1/2} t - \varphi) \tag{52}$$

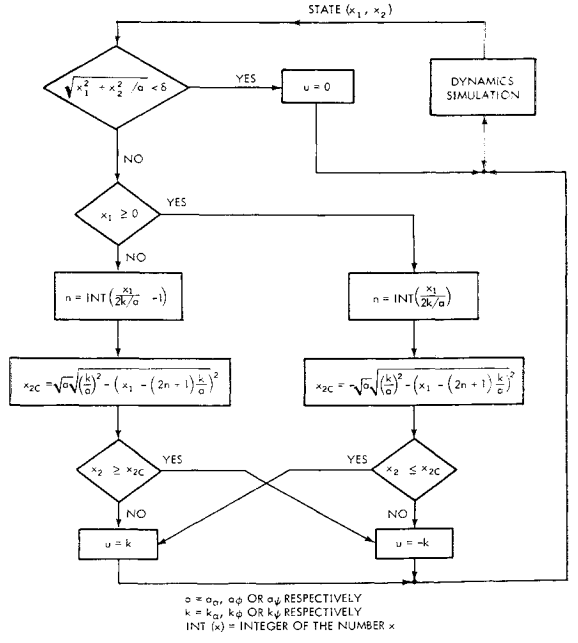

Fig. 3 Simplified flowchart for trajectories with optimal control according to Fig. 2 for GG coefficients a_α, a_ϕ, $a_\psi \neq 0$ and pointing to $x_1 = x_2 = 0$.

where A and φ are integration constants. Substituting Eq. (51) into Eq. (49) leads to the following solution of Eq. (47):

$$x_1(t) \mp k_\alpha a_\alpha^{-1} = (x_{10} \pm k_\alpha a_\alpha^{-1}) \cos a_\alpha^{1/2} t + x_{20} a_\alpha^{-1/2} \sin a_\alpha^{1/2} t \quad (53)$$

and

$$x_2(t) a_\alpha^{-1/2} = -(x_{10} \mp k_\alpha a_\alpha^{-1}) \sin a_\alpha^{1/2} t + x_{20} a_\alpha^{-1/2} \cos a_\alpha^{1/2} t \quad (54)$$

where

$$x_{10} = x_1(t = 0)$$

and

$$x_{20} = x_2(t = 0) = \dot{x}_1(t = 0)$$

It can be seen that $x_1(t)$ and $x_2(t)a_\alpha^{-1/2}$ form a circle whose center in the $x_1(t) - x_2(t)a_\alpha^{-1/2}$ plane lies at $x = k_\alpha/a_\alpha$ for $u_\alpha = k_\alpha$, and at $x = -k_\alpha/a_\alpha$ for $u_\alpha = -k_\alpha$.

Now the techniques found in Refs. 5, 7, and 10 can readily be applied. These lead to the known switching circles depicted in Fig. 2. This figure also includes an example of an optimal trajectory starting at $x_{10} = \alpha(t = 0)$ and $x_{20} = \dot{\alpha}(t = 0)$.

Optimal Control Laws for Roll (ϕ) and Yaw (ψ) with No Disturbance Torques

When Eqs. (34–36) are compared, no difference in their form is noted as long as $a_\psi \neq 0, a_\phi \neq 0$, and $a_\alpha \neq 0$. This is valid for a spacecraft with different principal moments of inertia. Therefore, for this case the same optimal control law can be applied to roll and yaw as is derived for pitch; this is obtained by substituting (a_α, k_α) by (a_ϕ, k_ϕ) or (a_ψ, k_ψ), respectively. However, another control law must be derived when two or three of the principle moments of inertia are equal. This will be done in the next section for yaw, when $I_{yy} = I_{zz}$.

The flow chart of a digital program for the control laws developed is given in Fig. 3. In this program a deadband is defined as

$$\delta = [x_1^2 + x_2^2/a_i]^{1/2} \quad (55)$$

with $a_i = a_\alpha$, a_ϕ or a_ψ, respectively.

Optimal Control Law for Yaw (ψ) for $I_{yy} = I_{zz}$ with No Disturbance Torques

For a symmetrical spacecraft $I_{yy} = I_{zz} \gg I_{xx}$ and hence a_ψ becomes 0. For this case another optimal control law must be derived for yaw (ψ): let

$$x_1 = \psi, x_2 = \dot{\psi} \quad (56)$$

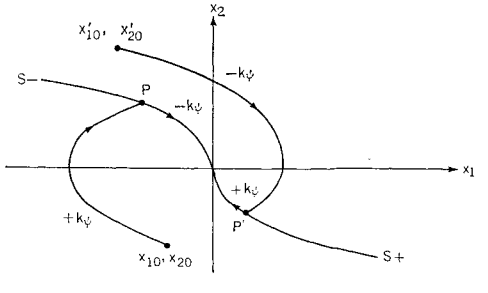

Fig. 4 Switching lines S_+ and S_- for optimal control of $x_1 = \psi$ and $x_2 = \dot{\psi}$ in the case of $a_\psi = 0$. Two examples of optimal trajectories are shown with switching points P and P', respectively. S_+ is given by $x_2 = -(2k_\psi|\psi|)^{1/2}$ S_- by $x_2 = +(2k_\psi|\psi|)^{1/2}$.

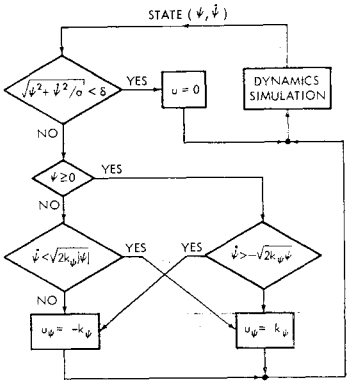

Fig. 5 Simplified flowchart for optimal control of yaw (ψ) for $a_\psi = 0$ using the scheme presented in Fig. 4. Similar explanations hold as for Fig. 3.

then (34) becomes

$$\dot{x}_1 = x_2, \dot{x}_2 = u_\psi \quad (57)$$

Using Eqs. (43) and (56), the Hamiltonian becomes $H = p_1 x_2 + p_2 u_\psi$, which is maximized by

$$u_\psi = k_\psi \operatorname{sgn} p_2$$

Applying Eq. (44),

$$\dot{p}_1 = 0, \dot{p}_2 = -p_1 \quad (58)$$

which results in

$$p_1 = B, p_2 = -Bt + C \quad (59)$$

From Eqs. (57) and (59) one obtains

$$x_1 = k_\psi (t^2/2) \operatorname{sgn}(C - Bt) + Dt + E \quad (60)$$

$$x_2 = k_\psi t \operatorname{sgn}(C - Bt) + D \quad (61)$$

Thus, all trajectories are parabolas. From Eq. (59) it is evident, that p_2 can change sign at the most once. Therefore, the complete optimal trajectory from a given initial condition in the $x_1 - x_2$ plane consists of one or two segments of a parabola, where the second parabola leads to the origin. It is evident, that the parabolas leading to the origin are also the switching lines (Fig. 4 and Refs. 5 and 6).

For initial conditions with $x_{20} = 0$ the time needed to reach the origin can be calculated to be $\tau = 2(x_{10}/k_\psi)^{1/2}$.

Figure 5 shows the flow chart for a digital computer program implementing this control law.

Stabilization to an Arbitrary Attitude

The foregoing optimal control laws lead $\alpha, \dot{\alpha}, \phi, \dot{\phi}, \psi$, and $\dot{\psi}$ to the origin. We will now consider stabilization or control to specified (set) values $\alpha_s, \phi_s, \psi_s \neq 0$ and to $\dot{\alpha} = \dot{\phi} = \dot{\psi} = 0$. Considering Eqs. (34–36) with $a_\alpha, a_\phi, a_\psi \neq 0$ the following new equations can be written, which contain an additional control term to balance the GG torque at the set value:

$$\ddot{\psi} + a_\psi \psi = \pm k_\psi + a_\psi \psi_s \quad (62)$$

$$\ddot{\phi} + a_\phi \phi = \pm k_\phi + a_\phi \phi_s \quad (63)$$

$$\ddot{\alpha} + a_\alpha \alpha = \pm k_\alpha + a_\alpha \alpha_s \quad (64)$$

But Eqs. (62–64) also can be written as

$$\ddot{\psi}_1 + a_\psi \psi_1 = \pm k_\psi, \ddot{\phi}_1 + a_\phi \phi_1 = \pm k_\phi$$

$$\ddot{\alpha}_1 + a_\alpha \alpha_1 = \pm k_\alpha$$

where $\psi_1 = \psi - \psi_s, \phi_1 = \phi - \phi_s$ and $\alpha_1 = \alpha - \alpha_s$. Therefore, Eqs. (42–54) can be applied as before, now leading ψ_1, ϕ_1, and α_1 to 0 and therefore, ψ, ϕ, and α to the desired setpoints. As in Fig. 2 switching lines and optimal trajectories

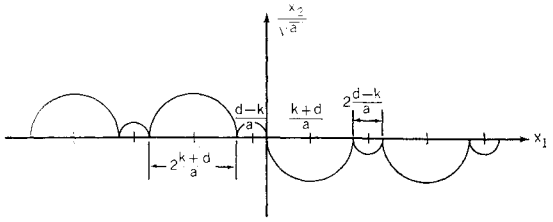

Fig. 6 Switching lines for optimal control of a, ϕ, or ψ in the case of a_a, a_ϕ, or $a_\psi \neq 0$, respectively, and in the presence of a constant disturbance torque. $x_1 = a$, ϕ or ψ, $x_2 = \dot{a}$, $\dot{\phi}$ or $\dot{\psi}$, $k = k_a$, k_ϕ or k_ψ, $a = a_a$, a_ϕ or a_ψ and $d = d_a$, d_ϕ or d_ψ, respectively.

can be constructed. They will appear shifted in direction of the x_1 axis when compared with Fig. 2 in order to lead to the set-points. A similar approach is valid for yaw (ψ) when $a_\psi = 0$. The switching lines of Fig. 4 must be shifted so that they lead to ψ_s.

Consideration of Disturbances

Two types of disturbances which should be considered are a constant bias torque and a disturbance torque with a 24-hr period. The former can be caused by misalignments of station-keeping thrusters; the latter, by solar pressure acting on the synchronous spacecraft. First a constant disturbance torque will be considered. In Eq. (36), d_α is the constant disturbance torque divided by I_{zz}. There are two approaches to solve this problem. First d_α could be measured by observing the shift of the trajectories and then counteracted by a control torque of the same magnitude. The total reduced control torque would be

$$u_\alpha = T_{cz}/I_{zz} = \pm k_\alpha - d_\alpha \tag{65}$$

This would lead to the same switching lines for optimal control as in Fig. 2. However, practical hardware considerations show that control torques according to Eq. (65) are much more difficult to implement than control torques of the form $u_\alpha = \pm k_\alpha$. Therefore, a modification of the switching lines of Fig. 2 is found as follows: From Eq. (36) one proceeds as was done for Eqs. (42-54):

$$\dot{x}_1 = x_2, \dot{x}_2 = -a_\alpha x_1 + u_\alpha + d_\alpha \tag{66}$$

and

$$H = p_1 x_2 + p_2(-a_\alpha x_1 + u_\alpha + d_\alpha) \tag{67}$$

which again results in condition (49). Replacing $\pm k_\alpha$ by $\pm k_\alpha + d_\alpha$ in Eqs. (53) and (54) shows that all trajectories are shifted by d_α/a_α in the direction of the x_1 axis and that the radii change. Similar considerations which led to Fig. 2 give Fig. 6 for the optimal switching lines.

Similar considerations hold for optimal control of ψ when $a_\psi = 0$. We only have to replace $\pm k_\psi$ by $\pm k_\psi + d_\psi$ in Eqs. (60) and (61). The equations for the switching lines read now

$$x_2 = [2(-k_\psi + d_\psi)x_1]^{1/2} \text{ for } x_1 \leq 0 \tag{68}$$

and

$$x_2 = -[2(k_\psi + d_\psi)x_1]^{1/2} \text{ for } x_1 \geq 0 \tag{69}$$

It is obvious that the preceding calculations are valid only for $k_i > d_i$ for $i = \alpha, \phi, \psi$.

For slowly changing disturbances optimal control could be implemented by changing the switching lines according to Fig. 6 and according to the present value of d_i. The interactions of changing disturbances and changing of switching lines bring up serious problems of identification of disturbances and problems of stability, which are presently under investigation. Two approaches to optimal control while the disturbance torque is varying are shown in Fig. 7. It is assumed that the optimal trajectory starts without disturbance at $x_{10}, x_{20}/a^{1/2}$ and reaches S_+§ and P_1 and follows S_+ (after switching control from $-k$ to $+k$) until a disturbance d occurs at the instant the state is at P_2. The trajectory now changes from that of S_+ to S_{d+}, where S_{d+} depends upon the disturbance. The S_{d+} trajectories are circles with their origin shifted by d/a in direction of x. Two procedures now exist: a) retention of $+k$ at P_2, thereby following trajectory R_{d+} to P_3 and there switching to $-k$. When S_{d+} is reached at P_4, control is switched back to $+k$ and S_{d+} followed to the origin, or b) after occurrence of the disturbance d at P_2, control is switched immediately to $-k$, until S_{d+} is reached at P_3'. S_{d+} then is followed to the origin by changing the control back to $+k$.

However, for the further investigations of the optimal control law in this paper it is assumed that $|T_d| \ll k$ for all three axes. Thus, it is not necessary to apply the refined control law given in Figs. 6 and 7. The approach to the origin in presence of small disturbances can be seen from Fig. 8.

The positive x_1 axis may serve as an additional switching line when the trajectory intersects from the negative x_2 direction. The negative x_1 axis forms the additional switching line in the case when the trajectory intersects coming from positive x_2 values. A more sophisticated control law in the presence of disturbances is suggested for future work in this area as follows: in order to guarantee stability (i.e., the distance from the set point shall be decreased at every instant of time) switching from $+k$ to $-k$ or vice versa shall also be implemented when the distance from the set point starts to increase.

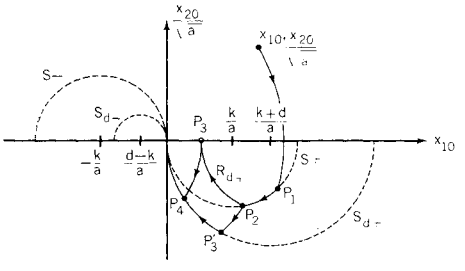

Fig. 7 Optimal trajectories under the influence of changing disturbances. The optimal trajectory starts at $(x_{10}, x_{20}\, a^{-1/2})$ without disturbance. A disturbance d occurs when the state is at P_2. The switching lines S_+ and S_- are then replaced by S_{d+} and S_{d-}, respectively. Two possible control procedures that lead the state to the origin are a) a policy that yields the path P_2, P_3, P_4, origin, or b) a policy that yields the path P_2, P_3', P_4, origin. For k, a, d, x_1, and x_2 see Fig. 6.

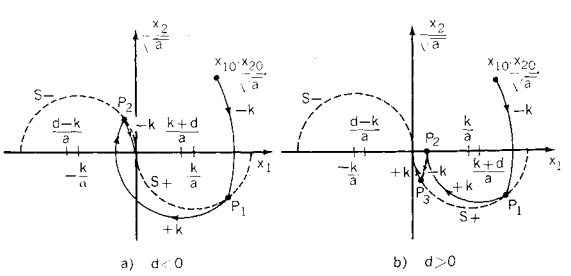

Fig. 8 Trajectories in the presence of small disturbances with switching lines as in Fig. 2; P_i—switching points. For k, a, d, x_1, and x_2 see Fig. 6.

§ S_+, replaces S_0, S_- replaces S_{-1} used earlier.

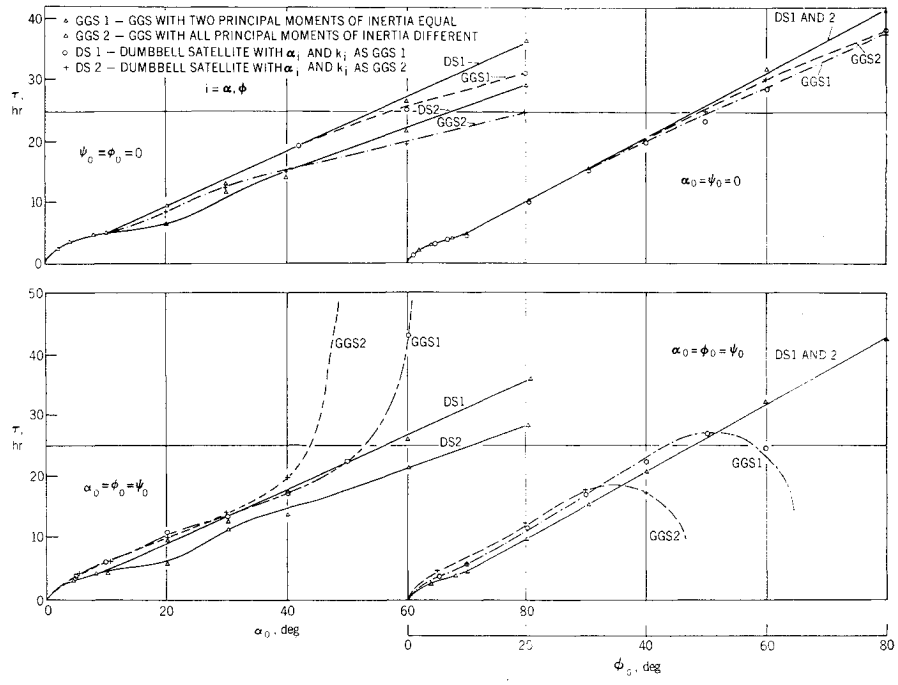

Fig. 9 Comparison of time consumed (τ) for damping of α_0 or ϕ_0 to 0°. $\dot{\alpha}_0 = \dot{\phi}_0 = \dot{\psi}_0 = 0$.

Application of the DS-Optimal-Control to the GGS

Two GGS configurations are used; GGS 1 is characterized by $I_{yy} = I_{zz} \gg I_{xx}$ and no damping mechanism, and GGS 2 is characterized by the moments of inertia of the ATS-D satellite. For the symmetric case (GGS 1)

$$[I] = \begin{bmatrix} 1000 & 0 & 0 \\ 0 & 48000 & 0 \\ 0 & 0 & 48000 \end{bmatrix} \text{slug-ft}^2$$

and $I_l = 0$ and $C_1 = C_2 = 0$. For the unsymmetric case (GGS 2)

$$[I] = \begin{bmatrix} 3180 & 0 & 0 \\ 0 & 13600 & 261 \\ 0 & 261 & 16700 \end{bmatrix} \text{slug-ft}^2$$

$I_l = 540$ slug-ft^2, $\rho_1 = 53.4°$, $C_1 = 1.322$ slug-ft^2/sec and C_2 4.7×10^{-2} slug-ft^2/sec^2. A necessary condition for controllability of a GGS is that in the whole pointing region for each axis,

$$T_c \geq |T_{gg}| + |T_d| \tag{70}$$

where T_c is the control torque exerted by the ion thruster, T_{gg} is the restoring torque due to the GG effect for a particular set of values, and T_d is the disturbance torque. To point in a particular direction α,ϕ,ψ, a certain T_{gg} has to be counteracted; this torque can be calculated by Eqs. (26–28). Since T_{gg} changes only when the set values of α,ϕ, and ψ are changed and therefore, much less often than T_d, counteraction of T_{gg} by a control torque of the same magnitude can be assumed. Pointing is desired to every point on the Earth as seen from a synchronous spacecraft. Therefore, $-8.5° \leq \alpha,\phi \leq 8.5°$ is valid, and a maximum T_{gg} in this region for the pitch (α) – axis of the asymmetric spacecraft is given by $T_{gg\alpha\max} = 2.5 \times 10^{-5}$ ft lb.

A disturbance torque is assumed to be caused by solar pressure with a peak value of 10^{-5}ft lb. Equation (70) now yields $T_{c\alpha} = \pm 35 \times 10^{-6}$ft lb. To obtain directly comparable results for the other axes of GGS 2 and for all axes of GGS 1, the same $k = T_c/I$ is chosen in every case. This results in: $T_{c\phi} = \pm 28.5 \times 10^{-6}$ft lb and $T_{c\psi} = \pm 6.6 \times 10^{-6}$ft lb for GGS 2, and $T_{c\alpha} = T_{c\phi} = \pm 10^{-4}$ft lb and $T_{c\psi} = \pm 2.09 \times 10^{-6}$ft lb for GGS 1.

The optimal switching lines given in Figs. 2 and 4 are applied to all three axes simultaneously. To compare the results obtained for a GGS with the idealized case of a DS, the time consumed for reaching an angle of 0° after a certain initial condition is plotted in the upper part of Fig. 9. For α_0 the time consumed for a DS is calculated by applying the optimal control law derived for the DS to the equation $\ddot{x} + ax = u$ where $a = a_\alpha$ and $u = \pm K_\alpha$. Two different a_α, called $a_{\alpha 1}$ ($=2.08 \times 10^{-8}$ sec^{-2}) and $a_{\alpha 2}$ ($=0.988 \times 10^{-8}$ sec^{-2}) are used for GGS 1 and GGS 2, respectively. Therefore, two different DS's must be used for comparison. DS 1 uses $a_{\alpha 1}$, whereas DS 2 uses $a_{\alpha 2}$. The lower time consumed by a GGS for higher initial conditions can be explained as follows: the coupling of all three axes transfers some of the energy of the pitch axis to roll and yaw axes where optimal control is also being applied. Therefore, energy is taken out of the whole system faster than for the uncoupled case of a DS. The region of α_0 between 10° and 43° for GGS 2 shows on the other hand, that this effect is out-weighed by the less exact approximation of an asymmetric GGS by a DS. Therefore a slightly higher time is consumed for this region than is predicted.

Corresponding calculations have been carried out for ϕ_0 with $a_{\phi 1} = 2.08 \times 10^{-8}$ sec^{-2} for GGS 1 and $a_{\phi 2} = 2.11 \times 10^{-8}$ sec^{-2} as well as for the corresponding DS's. The results are given in the upper part of Fig. 9. Similar explanations for the shape of the plot hold as for pitch.

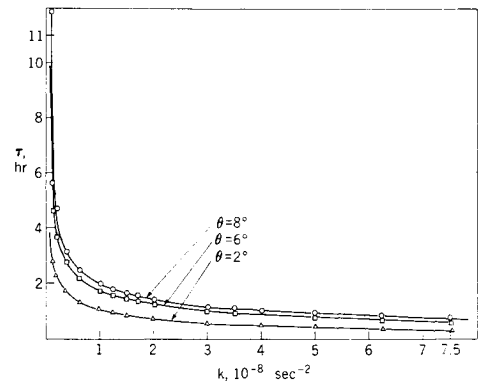

Fig. 10 Time consumed for changing the direction of pointing by θ($= \theta_\alpha$ or θ_ϕ) = 2°, 6°, and 8° as a function of the reduced torque $k = T_c/I$.

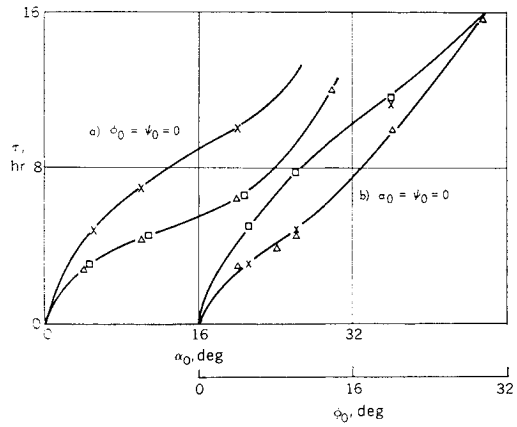

Fig. 11 Influence of disturbances on τ for GGS 2. The disturbances are sinusoidal with a peak value of 10^{-5} ft lb, a period of 24 hr and a phase of 0° (marked by □) or 180° (marked by x) relative to the last start of control action. △—DS.

Since the yaw angle is not significant for pointing to certain points on the surface of the Earth, graphs for yaw are not given here. It is mentioned, however, that for GGS 1, consistency with predicted values is achieved, whereas for GGS 2 some deviations from predicted values are observed. An exact explanation of this problem would involve a discussion of the exact Eqs. (1–21) and goes beyond the scope of this paper.

The lower part of Fig. 9 shows the influence on settling time τ of changing the initial conditions to $\alpha_0 = \phi_0 = \psi_0 \neq 0$ and $\dot{\alpha}_0 = \dot{\phi}_0 = \dot{\psi}_0 = 0$.

Figure 10 shows the effect on τ vs k for pointing to angles α_s, ϕ_s other than 0°. The simulations show that application of the control law for reference values $\neq 0$ gives no difference in τ when pointing to set values α_s, ϕ_s other than $\alpha_s = \phi_s = 0°$. This assumes that $\theta_\alpha = \alpha_0 - \alpha_s$ or $\theta_\phi = \phi_0 - \phi_s$ now has the same value as ϕ_0 or α_0, respectively, in Fig. 9. This assumed further that the same control torque T_c is still available and that the torque necessary to counteract the GG torque T_{gg} at the set value is supplied in addition to T_c; τ is increased if T_{gg} is counteracted by control torque while decreasing the torque T_c available for actual control purposes.

The case of control under the influence of a sinusoidal disturbance torque with a 24-hr period was investigated. The peak value of T_d is assumed to be 10^{-5}ft lb; τ is plotted in Fig. 11 for pitch ($\alpha_0 \neq 0, \phi_0 = \psi_0 = 0$) and for roll ($\phi_0 \neq 0, \alpha_0 = \psi_0 = 0$), with $\dot{\alpha}_0 = \dot{\phi}_0 = \dot{\psi}_0 = 0$ in both cases. Two phases for the disturbance torque are chosen, the first is 0° and the second is 180° relative to the starting point of control application. It can be seen that for favorable phases of the disturbance torque, there is no increase of τ, but under unfavorable circumstances τ is increased by 50%. (One can also consider cases where τ could be decreased.)

Closing Remarks

It has been shown that the time-optimal control law for a DS can be applied to a GGS as suboptimal control. The range of consistent results obtained for the GGS and for the DS depends on the initial conditions, on the GGS moments of inertia and on the disturbances. For initial conditions $\neq 0$ on only one GGS axis, the DS results are good approximations up to 80° with exact consistency up to 30° for roll and depending on the GGS moments of inertia, up to 10°–43° for pitch. For equal initial conditions $\neq 0$ and equal on all three GGS axes the DS results are good approximations up to 40–50°, depending on the GGS moments of inertia. Disturbances in some cases can help the control action but generally will extend control time.

References

[1] Barrett, C. C., "The Development of a Mathematical Model and a Study of One Method of Orbit Adjust and Station Keeping Gravity-Oriented Satellites," TND-3652, Nov. 1966, NASA.

[2] Roberson, R. E., "Attitude Control of Satellites and Space Vehicles," *Advances in Space Sciences*, Vol. 2, Academic Press, New York, 1960, pp. 351–436.

[3] Isley, W. C., "Optimal Control Application for Electrothermal Multijet Systems on Synchronous Earth Spacecraft," *Journal of Spacecraft and Rockets*, Vol. 5, No. 12, Dec. 1968, pp. 1444–1451.

[4] Frick, R. H., "Perturbations of a Gravity Gradient Stabilization System," Rept. AD 623279, Sept. 1965, The Rand Corp., Santa Monica, Calif.

[5] McCausland, I., *Introduction to Optimal Control*, Wiley, New York, 1969.

[6] Jones, G. S., Strauss, A., and Zvego, G. P., "Mathematical Aspects of Control Theory and the Problem of Satellite Attitude Control," Final Rept., Contract NAS 5-9172, Jan. 1966, NASA.

[7] Athans, M. and Falb, P. L., *Optimal Control*, McGraw-Hill, New York, 1966.

[8] Flügge-Lotz, I. and Craig, A., "The Choice of Time for Zeroing a Disturbance in a Minimum-Fuel Consumption Control Problem," ASME *Journal of Basic Engineering*, March 1965, pp. 29–38.

[9] *ATS-5 Data Book*, NASA Goddard Space Flight Center, Greenbelt, Md., 1969.

[10] Pontryagin, L. S. et al., *The Mathematical Theory of Optimal Processes*, Pergamon Press, Oxford, England, 1964.